*Desalination and Water Treatment*
www.deswater.com

doi: 10.5004/dwt.2021.27411

230 (2021) 384–399
August

# Influence of important parameters on the adsorption of diclofenac sodium by an environmentally friendly eucalyptus wood biochar and optimization using response surface methodology

Renata Treméa[a,*], Heloise Beatriz Quesada[b], Rosangela Bergamasco[b], Fatima de Jesus Bassetti[a]

[a]*Department of Chemistry and Biology, Federal University of Technology – Paraná – UTFPR, Curitiba 81280-340, Parana, Brazil, Tel. +55-41-3279-6800; emails: tremearenata@gmail.com (R. Treméa), bassetti@utfpr.edu.br (F. de Jesus Bassetti)*
[b]*Department of Chemical Engineering, State University of Maringa, Maringa 87020-900, Parana, Brazil, Tel. +55-44-3011-4759; emails: heloisequesada@gmail.com (H.B. Quesada), ro.bergamasco@hotmail.com (R. Bergamasco)*

Received 9 January 2021; Accepted 6 May 2021

**ABSTRACT**

Diclofenac sodium is a pharmaceutical that is extensively prescribed and consumed worldwide. Consequently, its release into water bodies has become a global concern, as it poses ecotoxicity, leading to severe public health and environmental problems. A literature research was performed to find a low-cost adsorbent with cationic characteristics that could be used to remove anionic contaminants from water, such as diclofenac sodium. In view of the above, this work aimed to investigate diclofenac sodium (DFS) removal using eucalyptus wood biochar (EWB) through the adsorption process. EWB was characterized by various techniques to obtain information regarding its surface charge, morphology and functional groups. Scanning electron microscopy displayed a porous surface, and Fourier-transform infrared spectroscopy showed a notable number of functional groups on the EWB surface. Brunauer–Emmett–Teller presented an $A_{BET}$ of 619.35 $m^2$ $g^{-1}$ and the point of zero charge was 7.98. The influence of pH, contact time, initial concentration, and temperature of DFS were studied in batch tests. Box–Behnken design was used in surface response methodology to optimize the process conditions and obtain the maximum adsorption capacity, which was found to be 42.08 mg $g^{-1}$, reached in 6 h, showing a good performance. Kinetic data best fit the pseudo-second-order model and equilibrium data were in better agreement with the Sips model, indicating monolayer adsorption. The thermodynamic study demonstrated the adsorption process was spontaneous and endothermic. Considering the high efficiency evidenced in this study, low cost for production and the adsorbent being a renewable source, EWB is a promising material with the potential to remove DFS from water.

*Keywords:* Water treatment; Diclofenac sodium; Biochar; Adsorption; Box–Behnken design

## 1. Introduction

In recent decades, contamination of natural resources has become increasingly threatening to public health and the environment [1]. Various emerging contaminants such as pharmaceuticals, personal care products and veterinary drugs have been detected in surface water, groundwater and water supplies, posing threats to the environment due to their ability to cause various undesirable effects [2,3].

Amongst emerging contaminants, diclofenac sodium is a non-steroidal anti-inflammatory drug used worldwide

* Corresponding author.

1944-3994/1944-3986 © 2021 Desalination Publications. All rights reserved.

since it relieves analgesic, arthritic and rheumatic pain [4]. As an excessively used drug, diclofenac sodium (DFS) has been frequently found in the environmental matrix in surface water and groundwater at low concentrations [5]. Its presence is responsible for causing toxic effects on bacteria, algae, and several studies have also reported physiological changes in animals at low concentrations [6,7]. Thus, it is necessary to develop, study and search for more efficient methods to remove a pollutant such as DFS from water and wastewater.

Several treatment techniques can be used to reduce or even eliminate the presence of these contaminants in bodies of water and among them, techniques such as ozonation [8], membrane separation processes [9], advanced oxidation [10], coagulation [11], and biological degradation processes have been widely used for water and wastewater treatment. Although these methods have shown efficiency in contaminant removal, they have several drawbacks, such as toxic residual products [12]. On the other hand, the adsorption process is considered a promising technology for emerging contaminant removal due to its efficiency, simplicity, flexibility in operation and design, and economic affordability [13,14]. Besides that, the adsorption process meets the environmentally friendly requirements of green chemistry due to its low sludge production, low cost, non-toxic products and regeneration capability [15,16].

Many adsorbent materials have been used for contaminant removal, such as chitosan, zeolites, clay, and even waste and low-cost adsorbents such as sludge, fly ash, etc. [17]. Although different types of adsorbents have been studied, activated carbon and biochar are still outstanding alternatives to eliminate organic compounds [18,19]. Their characteristics involve great specific surface area, high porosity and adsorption capacity, the effectiveness of contaminant removal and low specificity [19,20].

Commercially available activated carbons have been utilized in several studies for water treatment, but these activated carbons may hinder the process due to their high cost [7]. Thus, for the purpose of reducing the use of high-cost activated carbons, the use of alternative adsorbent materials has been reported because of their high selectivity, great removal performance, and low cost [21]. Thus, biochar has emerged as an advantageous and environmentally friendly material, manufactured at low cost for many purposes, such as pollution minimization, climate change mitigation, bioenergy utilization and biomaterial waste management [22,23]. The alternative cheap materials searched for include peat, tree, eucalyptus barks, soil, rice husk, wood, etc [24].

The Brazilian forestry sector represents a worldwide reference and shows the highest wood productivity in the world. Amongst the 7.83 million ha of the total area of trees planted for industrial purposes, eucalyptus plantations occupy 5.7 million ha [25]. In Brazil, the unused agricultural waste products represent widely available and environmentally friendly materials that have great potential as adsorbents for water and wastewater treatment. Applying these waste products in adsorption processes allows a better management of them and helps find a solution for contaminant removal in the water system [21].

Despite the diversity of studies reported in the literature utilizing activated carbon to remove diclofenac sodium from water, the use of eucalyptus wood biochar has not yet been reported. In this sense, this study aimed to explore the adsorption of diclofenac sodium in aqueous solutions by batch testing, using eucalyptus wood biochar as an adsorbent. The adsorption process was investigated through pH effect, contact time, initial drug concentration, and temperature. Box–Behnken (BBD) in response surface methodology (RSM) was utilized to optimize the maximum adsorption capacity. Finally, kinetic, equilibrium and thermodynamic studies were performed.

## 2. Materials and methods

### 2.1. Reagents

Diclofenac sodium ($C_{14}H_{10}C_{l2}NNaO_2$) was purchased in Curitiba (Brazil) and Table S1 shows its characteristics and properties. Eucalyptus wood biochar was provided by Carbomafra SA. The material was crushed, sifted using a set of Tyler Sieves, and dried at 373 K for 24 h. Eucalyptus wood biochar (EWB) was used in this study with a particle size of 0.25 mm.

### 2.2. Adsorbent characterization

EWB was characterized by physicochemical and structural characteristics. The particle size was found by placing 20 g of EWB on a series of Tyler Sieves and mechanically shaking them for 5 min (Bertel VP-01). After this, the sieves were separated and the remaining EWB on each sieve was calculated. Finally, each adsorbent weight obtained was converted to a percentage of the total retained on each sieve.

Textural characterization was performed through $N_2$ adsorption/desorption isotherms at 77 K through a Quantachrome Gas Sorption Analyzer (Nova 2000) and the software NovaWin. The samples were degassed under vacuum at 363 K for 6 h. Brunauer–Emmett–Teller (BET) and Barrett–Joyner–Halenda methods were used to calculate the specific surface area and obtain the average pore volume and diameter, respectively.

Through scanning electron microscopy (SEM) Tescan VEGA3 LMU, it was possible to analyze the adsorbent morphology. The structural characteristics were studied and analyzed through X-ray diffraction (XRD) with the Shimadzu XRD-7000, performed in the 2θ ranging from 5° to 120°, and Raman spectroscopy using the WITec Alpha 300R, with a wave excitement of 531.973 nm and integration time of 1.09. Fourier-transform infrared (FTIR) spectra were obtained to explore the chemical groups on EWB, using a Varian 640-IR, ranging from 400–4,000 $cm^{-1}$ and with a resolution of 4 $cm^{-1}$.

The point of zero charge ($pH_{pzc}$) was performed in accordance with the methodology proposed by Regalbuto and Robles [26], in which 50 mg of EWB was prepared and mixed with 50 mL of distilled water under various pH conditions (MS Tecnopon®) ranging from 2 to 12. For pH adjustments, HCl and NaOH 0.1 mol $L^{-1}$ solutions were used. The samples were agitated at 200 rpm for 24 h at 298 K and then centrifuged at a speed of 2,400 rpm for a period of

20 min. After this, the pH was measured again and the $pH_{pzc}$ was obtained through the plot of a $pH_{final} \times pH_{initial\text{-}final}$ graph.

### 2.3. Adsorption studies

The experiments were executed as batch studies. Diclofenac sodium stock solution (100 mg $L^{-1}$) was prepared in ultrapure water (MegaPure) and diluted to different concentrations for the experiments. After this, 50 mL of each DFS concentration was added to 100 mL amber bottles containing a certain amount of adsorbent. The mixtures were added into a thermostatic shaker (Tecnal TE-4200) for a predetermined time. The mixtures were centrifuged (Fanem – Baby I 206-BL) at 2,400 rpm for 20 min and the samples were quantified in a UV-Vis spectrophotometer (Global Trade Technology UV-5100) at 279 nm.

#### 2.3.1. Influence of pH

The effect of pH was tested adjusting different pH conditions from 4 to 9 in the solution containing the pharmaceutical (10 mg $L^{-1}$), utilizing 20 mg of EWB. The experiment was conducted for 6 h at 298 K.

#### 2.3.2. Influence of contact time

To study how the contact time influences the process, 20 mg of EWB was added in a 10 mg $L^{-1}$ DFS solution. The experiment was conducted with different contact times (from 0.5 to 12 h) at 298 K and the best pH condition was previously found.

#### 2.3.3. Experimental design

The RSM by Box–Behnken design (BBD) was conducted to optimize three operation parameters: speed rate (rpm), initial DFS concentration (mg $L^{-1}$) and adsorbent dosage (mg), to maximize the DFS uptake. Each variable was varied at three levels (–1, 0 and +1), indicating low, medium and high. The BBD matrix is shown in Table 1. A total of 15 experiments were designed in this research using Eq. (1).

$$N = 2k\left(k-1\right) + C_p \tag{1}$$

where $N$ is the number of experiments, $k$ is the number of variables and $C_p$ is the number of center points.

The experimental results were fit to a second-order polynomial equation that describes the response surface and expresses the variables' interactions. The 3D surface plots were used to analyze the adsorption performance and analysis of variance (ANOVA) tests were performed to analyze the significance of the model [22]. The statistical tests were performed through the software Minitab® 19.

After the experiments were performed, the best adsorbent dosage, pH, contact time, stirring rate and initial drug concentration were chosen to conduct the following experiments for the modeling studies.

#### 2.3.4. Influence of initial DFS concentration and temperature

To perform this test, 10 mg of EWB was mixed with the DFS solution containing different concentrations (3–21 mg $L^{-1}$) at various temperatures (295, 305 and 315 K). The experiment was evaluated using the best conditions from the previous studies and the best conditions obtained in BBD.

### 2.4. Adsorption modeling

Kinetic, equilibrium and thermodynamics were investigated through adsorption modeling to explain the characteristics and behavior of DFS removal by EWB. The samples were agitated during different contact times (0.5–12 h) at 185 rpm and 10 mg of EWB was mixed using 15 mg $L^{-1}$ DFS solution at natural pH (5.5) and 298 K.

The isotherms were analyzed at three temperatures (295, 305 and 315 K) under the agitation of 185 rpm for 6 h, varying the initial drug concentration (2–20 mg $L^{-1}$) at natural pH and 10 mg of EWB. Origin® 2016 was utilized for data fitting. Eqs. (2) and (3) were used to calculate the adsorption capacities ($q_t$ and $q_e$ mg $g^{-1}$).

$$q_t = \frac{\left(C_0 - C_t\right)}{m} v \tag{2}$$

$$q_e = \frac{\left(C_0 - C_e\right)}{m} v \tag{3}$$

where $C_0$ and $C_e$ (mg $L^{-1}$) are the initial ($t$ = 0) and equilibrium DFS concentration; $v$ (L) represents the solution of the volume and $m$ (mg) is the mass of EWB.

The adsorption process was investigated through kinetic models: pseudo-first-order (PFO) [Eq. (4)] [27], pseudo-second-order (PSO) [Eq. (5)] [28] and intraparticle diffusion (ID) [Eq. (6)] [29].

$$q_t = q_e\left(1 - e^{-k_1 t}\right) \tag{4}$$

$$q_t = \frac{q_e^2 k_2 t}{1 + q_e k_2 t} \tag{5}$$

Table 1
Independent variables and their levels for BBD

| Independent variables | Symbol | Levels | | |
|---|---|---|---|---|
| | | Low (–1) | Center point (0) | High (+1) |
| Stirring rate (rpm) | $X_1$ | 100 | 150 | 200 |
| Drug concentration (mg $L^{-1}$) | $X_2$ | 5 | 10 | 15 |
| Adsorbent dosage (mg) | $X_3$ | 10 | 20 | 30 |

$$q_t = k_{id} t^{0.5} + C \quad (6)$$

where $q_t$ and $q_e$ (mg g$^1$) are the quantity of DFS adsorbed per unity of mass at the established time and at equilibrium, respectively; $k_1$ (h$^{-1}$), $k_2$ (g mg$^{-1}$ h$^{-1}$) and $k_{id}$ (mg g$^{-1}$ h$^{0.5}$) are the pseudo-first-order, pseudo-second-order and intraparticle diffusion rate constants, respectively, and $C$ (mg g$^{-1}$) is the intercept associated with the thicker boundary layer.

For the equilibrium study, Langmuir [30], Freundlich [31], Sips [32] and Redlich–Peterson [33] isotherms were employed through Eqs. (7)–(10) to analyze the equilibrium characteristics of adsorption.

$$q_e = \frac{q_m K_L C_e}{1 + K_L C_e} \quad (7)$$

$$q_e = K_F C_e^{1/n_F} \quad (8)$$

$$q_e = \frac{q_{max} K_S C_e^{n_s}}{1 + K_S C_e^{n_s}} \quad (9)$$

$$q_e = \frac{K_{RP} C_e}{1 + \alpha_{RP} C_e^{\beta}} \quad (10)$$

where $C_e$ (mg L$^{-1}$) is the solution concentration at equilibrium; $q_m$ (mg g$^{-1}$) is the maximum adsorption possible; $K_L$ (L mg$^{-1}$), $K_F$ (mg g$^{-1}$)(mg L$^{-1}$)$^{1/nF}$, $K_S$ (L mg$^{-1}$), and $K_{RP}$ and $\alpha_{RP}$ (L mg$^{-1}$)$^{\beta}$ are the Langmuir, Freundlich, Sips, and Redlich–Peterson constants, respectively; $n_F$ and $n_S$ are Freundlich and Sips constants for heterogeneity. The closer $n_S$ is to zero, the more heterogeneous the system is ($0 \le n_S \le 1$) [34] and $\beta$ is the Redlich–Peterson exponent that lies between 0 and 1.

### 2.5. Thermodynamic study

Changes in the temperature can affect the nature of the process, along with its characteristics. The adsorption study was investigated at three temperatures (295, 305 and 315 K) through the thermodynamic parameters: Gibbs free energy change ($\Delta G$, kJ mol$^{-1}$), enthalpy change ($\Delta H$, kJ mol$^{-1}$) and entropy change ($\Delta S$, J mol$^{-1}$ K$^{-1}$). Both parameters were obtained by the following equations:

$$\Delta G = -RT \ln K \quad (11)$$

$$\ln(K) = \left( \frac{\Delta S^\circ}{R} - \frac{\Delta H^\circ}{R} \right) \frac{1}{T} \quad (12)$$

where $R$ (8.314 J mol$^{-1}$ K$^{-1}$) is the universal gas constant and $T$ (K) is the absolute temperature. The thermodynamic equilibrium constant (K) was calculated using the best-fit isotherm model, according to the methodology described by Lima et al. [35].

## 3. Results and discussion

### 3.1. Adsorbent characterization

EWB was characterized by the particle size, SEM, $N_2$ adsorption/desorption isotherm, BET, FTIR, XRD, Raman spectroscopy, and $pH_{pzc}$. Fig. S1 shows the particle size distribution. For 5 min, almost 50% of the total adsorbent

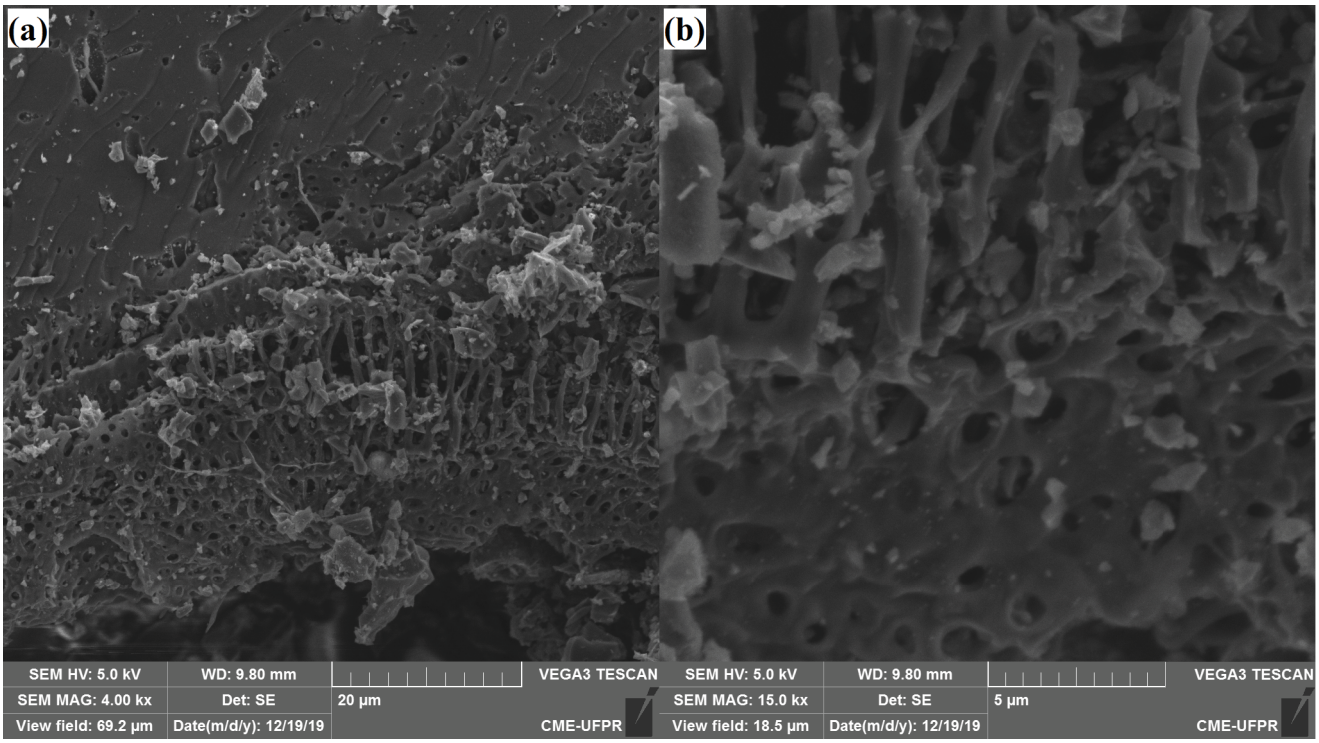


Fig. 1. SEM images of EWB at a (a) 20 µm and (b) 5 µm scale.

weight passed 250 mesh; hence, the adsorbent particle size used for the following experiments was 0.25 mm. Fig. 1 illustrates through the SEM images that EWB presented a porous structure distributed across the entire material surface and may be effective to remove DFS.

Through the analysis of XRD patterns for EWB (Fig. 2a), it was possible to observe the obvious amorphous structure exhibited by the typical diffraction bands at 23.78° and 44.08°, which belonged to (002) and (101) planes of graphitic carbon [36]. This agrees with the patterns shown in Raman spectroscopy (Fig. 2b), which exhibited a strong G band around 1,600 $cm^{-1}$ and a D band around 1,350 $cm^{-1}$, representing the graphitic and disordered structure, respectively [37].

Fig. 3a illustrates the FTIR spectra, revealing the chemical groups present on EWB. The high peak at a wavenumber of 3,464 $cm^{-1}$ indicates free and associated hydroxyl groups (O–H) in alcohols, carboxylic, water and phenolic compounds on the EWB surface [38,39]. The band at 2,364 $cm^{-1}$ indicates ketone structures present on EWB [40,41]. The peak at 1,637 $cm^{-1}$ is associated with C=C stretching vibrations in aromatic rings and C=O bond in the carboxylic acid group [42]. The band at 1,385 $cm^{-1}$ indicates C=C stretching vibrations in aromatic rings and CH bonding also contributes to this peak [43,44]. The characteristic peak at 1,115 $cm^{-1}$ consists of OH and/or C–O vibrations [40] and the bands at 461 and 613 $cm^{-1}$ are attributed to the external CH bonding of aromatic rings [41,45].

Fig. 3b shows the $N_2$ adsorption/desorption isotherm and Table 2 presents the pore size characteristics. EWB showed a high surface area (619.35 $m^2\ g^{-1}$) and a great size distribution of the pores, confirmed by SEM images (Fig. 1a and b). The $N_2$ adsorption/desorption isotherm showed high $N_2$ adsorption at low P/Po, indicating that EWB contains micropores [46]. However, according to Thommes et al. [47], it is also a type IVa isotherm with hysteresis, which means that the adsorbent is mesoporous, being in conformity with the pore characteristics shown in Table 2.

The surface charges present on the EWB surface were investigated through its $pH_{pzc}$. Fig. 3c illustrates the plot $pH_{final} \times pH_{initial\text{-}final}$, where EWB showed a $pH_{pzc}$ of 7.98. This means that the EWB surface presents negative charges for values below $pH_{pzc}$, and positive charges for values above $pH_{pzc}$.

### 3.2. Adsorption studies

#### 3.2.1. Influence of pH

Fig. 4 displays the study of the pH effect. DFS is considered a weak acid (pKa = 4.15) and poorly soluble in water in its unionized form [48]. This means that favorable interactions between EWB and DFS will occur for pH values between the $pH_{pzc}$ and the pKa. The adsorbent characteristics ($pH_{pzc}$ = 7.98) and the acidic characteristics of DFS (pKa = 4.15) indicate that DFS adsorption should be guaranteed for pHs below the adsorbent $pH_{pzc}$.

When the pH of a solution is below pKa, the DFS solubility in water decreases [49], so this experiment was performed ranging from pH 4 to 9. Fig. 4 shows that increasing the solution pH slightly decreases the DFS adsorption. According to Guerra et al. [50], this happens due to the increase in the negative charge of EWB, as well as the number of deprotonated functional groups on the surface, such as –COO– and –O– [50,51]. In this case, electrostatic repulsion occurring between the pharmaceutical and the EWB negative surface can be observed. Additionally, the acidic groups of EWB observed in FTIR spectra (Fig. 3a) could favor the interaction with the polar functional groups present in DFS [12]. Hydrogen bonding between the carboxylic group of EWB and negative species of DFS could be occurring in the process [12,52]. As it can be observed in Fig. 4a, the change of the adsorption capacity as the pH changes are low, which means that both hydrogen bonding and Van der Waals forces could be playing a significant role in the adsorption process [53,54]. Bernardo et al. [52] also reported a similar behavior between the pH condition and the DFS uptake. The highest adsorption

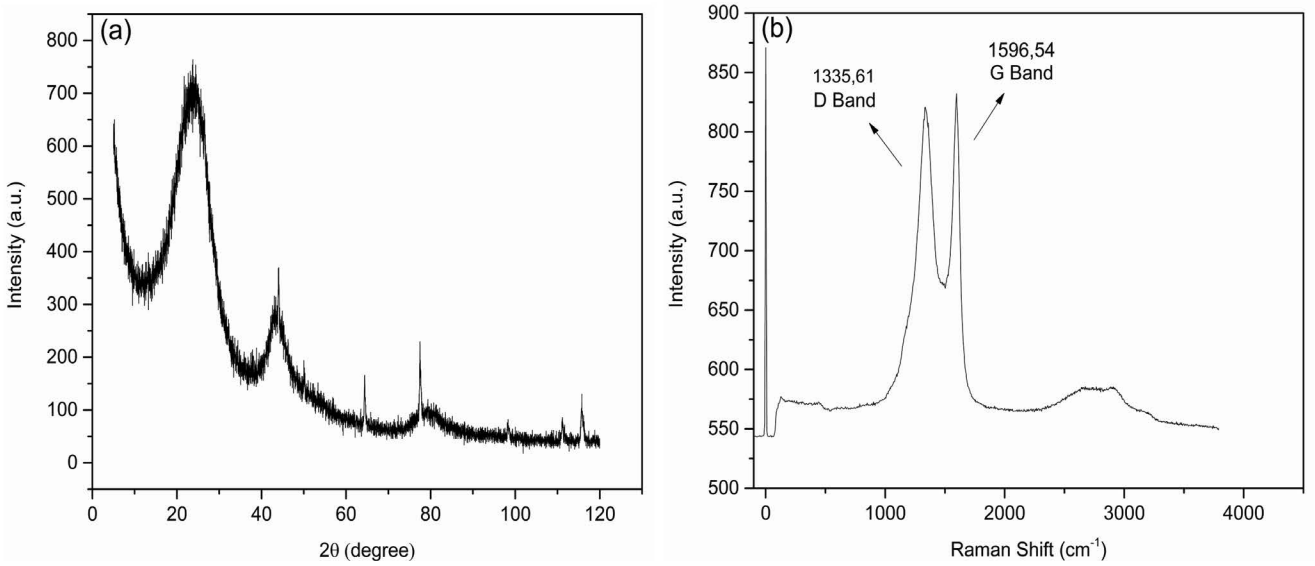


Fig. 2. (a) XRD patterns and (b) Raman spectra of the EWB sample.

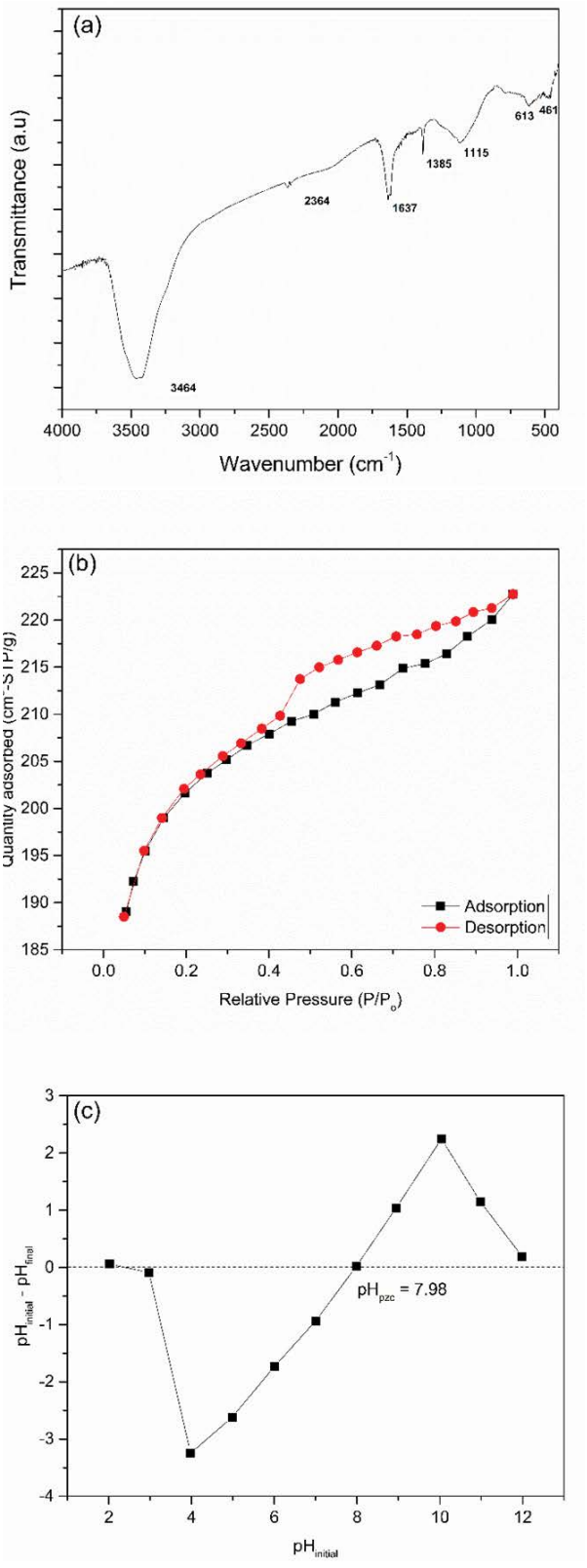


Fig. 3. (a) FTIR spectra of the EWB sample, (b) $N_2$ adsorption/desorption isotherms of the EWB sample and (c) $pH_{pzc}$ of the EWB sample at various pH conditions. Conditions: stirring rate = 200 rpm; temperature = 298 K; contact time = 24 h; adsorbent dosage = 50 mg.

Table 2
Textural characteristics of the EWB sample

| Adsorbent | EWB |
|---|---|
| $A_{BET}$ ($m^2\ g^{-1}$) | 619.35 |
| Average pore diameter (nm) | 3.617 |
| Pore volume ($cm^3\ g^{-1}$) | 0.036 |

capacity was recorded to be at pH 5, which is an approximate value to the natural pH of the DFS solution (5.5). Therefore, the natural pH was adopted for the following experiments.

### 3.2.2. Influence of contact time

Fig. 4b illustrates the influence of various contact times (0.5–12 h) on the DFS adsorption. It is possible to observe a notable increase in DFS uptake at the early stage. This behavior occurs because of the availability of active sites and a higher possibility of adsorption. As the process progressed, the increase was slower because the quantity of available sites decreased. The highest adsorption capacity was found to be 20.86 mg $g^{-1}$ when the system reached equilibrium after 6 h, which means that there is no longer mass transfer between the fluid phase and the adsorbed phase.

### 3.2.3. Experimental design

Table S2 displays coded variables with their predicted and actual response results. The independent factors were stirring rate ($X_1$), drug concentration ($X_2$) and adsorbent dosage ($X_3$), and their individual behavior and interactions were studied by the BBD. Other parameters such as temperature, contact time, and pH were fixated. The adsorption capacity was the response and it was investigated through those parameters. The model generated the final quadratic polynomial equation [Eq. (13)] and Table S3 presents the results for the analysis of variance (ANOVA) test.

$$\begin{aligned} DFS_{removal} = {} & -21.56 + 0.4212X_1 + 1.572X_2 - 0.252X_3 \\ & - 0.001245X_1^2 - 0.0521X_2^2 - 0.00023X_3^2 \\ & + 0.00369X_1X_2 - 0.00182X_1X_3 + 0.0074X_2X_3 \end{aligned} \quad (13)$$

The model was significant at a probability level of $p = 0.05$. ANOVA showed a high $R^2$ value (0.9912), implying that the developed model was accurate. This means that the regression model represented 99.12% of the experimental results and only 0.88% was not explained by this model [55]. The predicted vs. actual results plot for DFS uptake is depicted in Fig. S2. The plot showed a correlation coefficient of 0.9905, revealing a good correlation between the actual and predicted values. The predicted $R^2$ value (0.8658) and the adjusted $R^2$ (0.9754) were reasonably in agreement, indicating the reliability of the model [56]. Sood et al. [57] reported that the insignificant value of lack of fit (>0.05) is desirable because it reveals that terms left out of the model are not significant. The lack of fit value during this study was 0.081, suggesting that the developed model fit well.

Fig. 5 illustrates the three-dimensional (3D) response surface plots of DFS adsorption as a function of independent

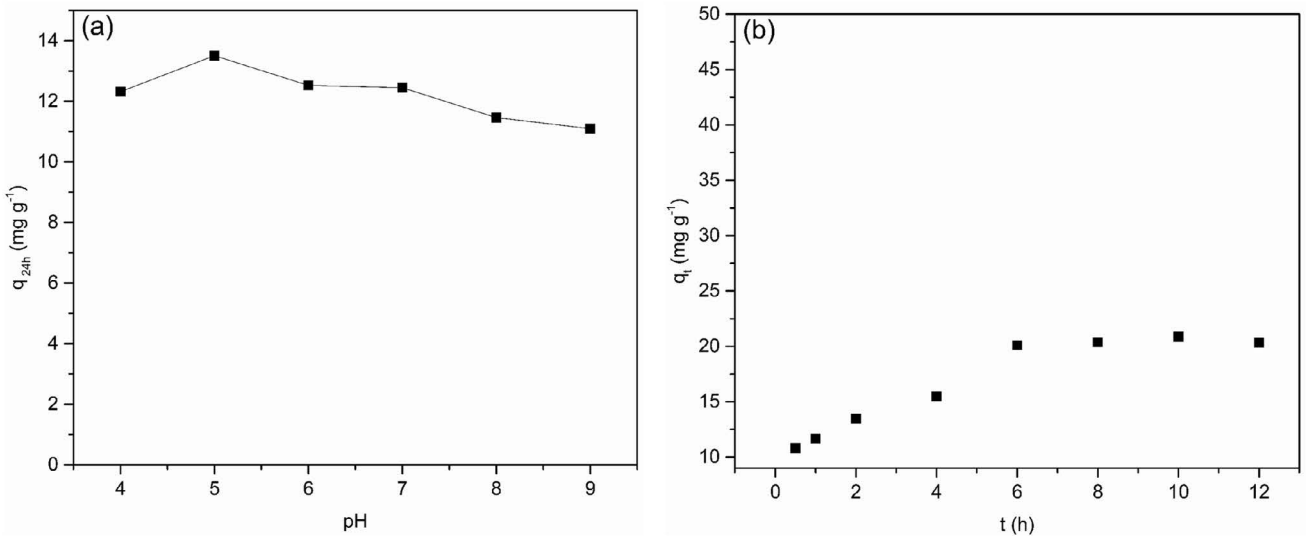


Fig. 4. (a) Effect of pH in 6 h of contact time and (b) contact time at pH 5.5 (natural) of DFS adsorption on EWB. Conditions: stirring rate = 200 rpm; initial DFS concentration = 10 mg L$^{-1}$; temperature = 298 K; adsorbent dosage = 20 mg.

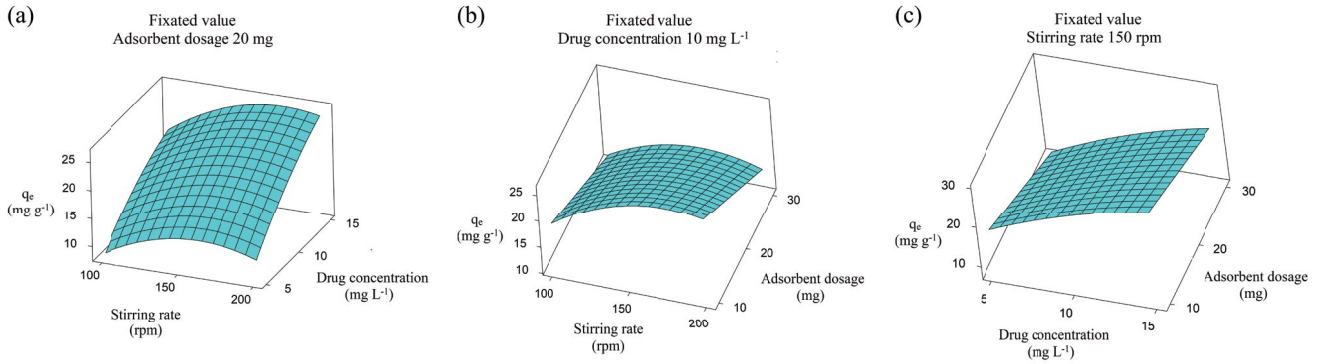


Fig. 5. 3D plots showing the effects of (a) stirring rate and drug concentration (b) stirring rate and adsorbent dosage and (c) drug concentration and adsorbent dosage in the DFS adsorption on EWB. Conditions: pH = 5.5 (natural); temperature = 298 K.

variables. The plot verifies the interactive 3D effects of the dependent variable (DFS adsorption capacity) and three independent variables (stirring rate, drug concentration and adsorbent dosage), in which one variable is set constant in its center point (0). Fig. 5a shows the DFS adsorption capacity in relation to the stirring rate and drug concentration, with a constant adsorbent dosage. The adsorption capacity increases from 9.31 to 24.77 mg g$^{-1}$ by increasing the stirring rate and drug concentration. This happens because the increase in the initial drug concentration requires a higher amount of the drug to be adsorbed, raising the driving force from the concentration gradient [58] and increasing the stirring speed, thus enhancing the homogeneity to the mixture [59].

Fig. 5b depicts the relationship of the DFS uptake as a function of stirring rate and adsorbent dosage, with a constant value of drug concentration. The DFS adsorption capacity increases with an increase in the stirring rate but with a decrease in the EWB dosage (from 11.39 to 25.23 mg g$^{-1}$). The adsorption capacity represents the quantity of the DFS adsorbed by EWB per unit mass. Therefore, it tends to increase by using a smaller amount of EWB, since raising the EWB dosage results in the instauration of the adsorbed sites [60,61]. Furthermore, interactions between the particles may occur, such as aggregation, which is a result of the high amount of adsorbent [60].

Finally, Fig. 5c shows the DFS adsorption capacity in relation to drug concentration and adsorbent dosage, with a constant stirring rate. The adsorption capacity increased from 7.17 to 30.51 mg g$^{-1}$ by increasing the concentration and decreasing the adsorbent dosage. This occurs because the solution contains a greater amount of adsorbate, which will fill all the available adsorbent sites, thus increasing the adsorption capacity. Hence, the maximum DFS uptake occurs for greater stirring rate and drug concentration, and for lower EWB dosage.

BBD and RSM were used to reveal the best conditions for the DFS uptake. The optimal conditions were 183.84 rpm for the stirring rate, 15 mg L$^{-1}$ for the drug concentration and 10 mg for the adsorbent dosage. These conditions showed a predicted adsorption capacity of 31.03 mg g$^{-1}$. A new experiment with the optimal conditions was conducted to validate the optimization and obtain the actual $q_e$

value (31.78 mg $g^{-1}$). Table S4 shows the optimal conditions and the actual $q_e$ value. The stirring rate was set to 185 rpm to benefit the process.

### 3.3. Adsorption study

#### 3.3.1. Kinetic study

The kinetic modeling study helps to investigate and analyze the efficiency for pollutant removal [62], adsorption dynamics and how time affects the process [63]. With the optimal conditions obtained from BBD in Section 3.2.3 – Experimental design, the second study of contact time was performed for the kinetic modeling.

The second study of contact time was performed in order to compare the adsorption capacity before and after the application of the Box–Behnken design. Fig. 6a shows similar behavior to the study depicted in Fig. 4b. There was a rapid uptake increase in the first 4 h, with an adsorption capacity of 35 mg $g^{-1}$, which was 2.16 times higher than the one witnessed in Fig. 4b for the experiment performed without the optimal conditions (15.48 mg $g^{-1}$). After reaching the equilibrium in 6 h, the adsorption capacity increased from 20.42 mg $g^{-1}$ without the optimal conditions (Fig. 4b) to approximately 43.98 mg $g^{-1}$ with the optimal conditions (Fig. 6a). Table 3 presents the kinetic parameters regarding PFO, PSO and ID.

The standard deviation of residues (SD) was used to help comprehend the fitness of each model by dividing the SD of each model by the SD of the minimum value. The lesser SD values indicate a smaller disparity between the theoretical and experimental $q$ values [64]. Fig. 6a and b illustrate the kinetic data regarding PFO, PSO and ID.

In Fig. 6a and Table 3, it is possible to observe that the $R^2$ coefficient and SD showed that the pseudo-second-order model best fit the data, with the greatest determination coefficient and the lowest SD amongst the models. A small difference can be noted between the experimental and calculated values for the adsorption capacity. This most possibly happens because, according to Wong et al. [65], boundary layer effects could be occurring during the process. However, the $R^2$ value is still higher and the SD value is lower for the PSO model, which indicates that the PSO model best fits the experimental data. Although PFO and PSO models are traditionally utilized in adsorption studies, the most limiting mechanisms are the ones related to diffusion, such as external diffusion, boundary layer or intraparticle diffusion [66]. The intraparticle diffusion model determines the adsorption rate-limiting step. If the ID model takes part in the process, then the plot $q_t \times t^{0.5}$ will be linear, and if the line passes through the origin ($C$ = 0), it means that this model controls the process [67].

Table 3
Kinetic parameters for DFS adsorption on EWB. Conditions: stirring rate = 185 rpm; initial DFS concentration = 15 mg $L^{-1}$; pH = 5.5 (natural); temperature = 295 K; adsorbent dosage = 10 mg

| Pseudo-first-order | | Pseudo-second-order | |
|---|---|---|---|
| $q_{exp}$ = 32.96 mg $g^{-1}$ | | | |
| $q_t$ (mg $g^{-1}$) | 32.27 | $q_t$ (mg $g^{-1}$) | 37.39 |
| $k_1$ ($h^{-1}$) | 0.5980 | $k_2$ (g $mg^{-1}$ $h^{-1}$) | $1.980 \cdot 10^{-2}$ |
| $R^2$ | 0.9405 | $R^2$ | 0.9789 |
| SD | 1.977 | SD | 1.178 |
| Intraparticle diffusion | | | |
| $k_{id1}$ (mg $g^{-1}$ $h^{-0.5}$) | 10.91 | $k_{id2}$ (mg $g^{-1}$ $h^{-0.5}$) | 1.142 |
| $C$ | 4.889 | $C$ | 29.41 |
| $R^2$ | 0.9449 | $R^2$ | 0.3195 |
| SD | 1.574 | SD | 0.5567 |

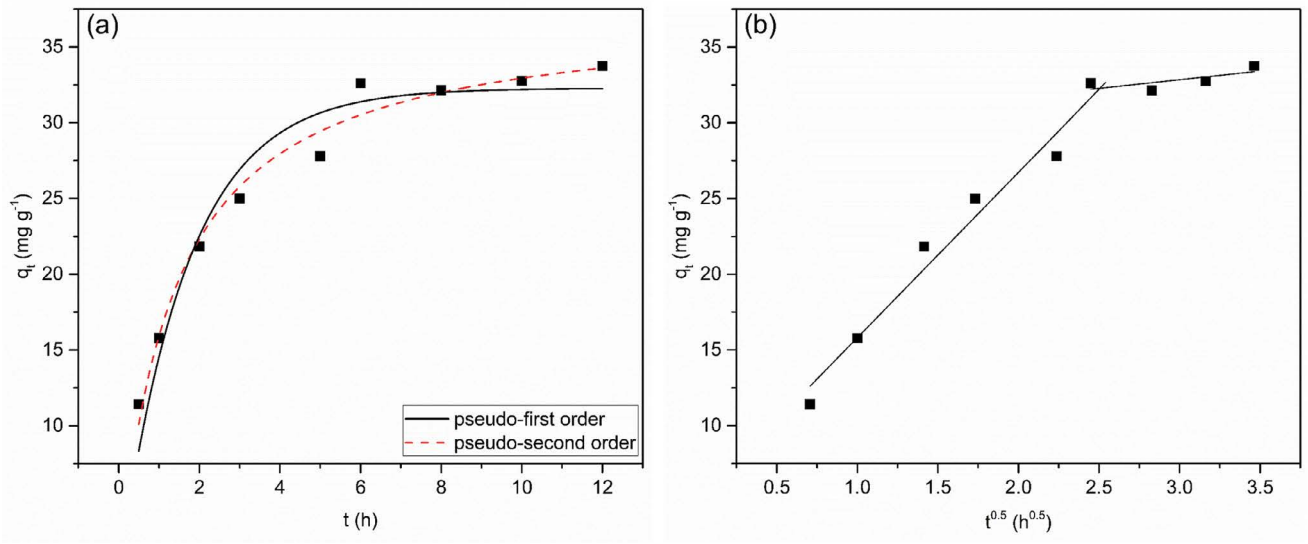


Fig. 6. Adsorption kinetic data for DFS on EWB for (a) pseudo-first-order and pseudo-second-order models and (b) intraparticle diffusion model graph of $q_t \times t^{0.5}$. Conditions: stirring rate = 185 rpm; initial DFS concentration = 15 mg $L^{-1}$; pH = 5.5 (natural); temperature = 295 K; adsorbent dosage = 10 mg.

The plot in Fig. 6b exhibited a multilinearity containing two linear regions with different slopes, suggesting multiple steps in the process. The first stage represents the transfer of molecules from bulk through the film of liquid containing a high initial DFS concentration and a vast number of available sites. Therefore, this is the fastest sorption stage [68]. The next stage involves intraparticle diffusion as the rate-determining step, so the process happens through small pores [69]. Besides, the regression line did not pass the origin ($C \neq 0$), indicating that ID is not the only rate-limiting step in this process [70].

### 3.3.2. Equilibrium study

According to Abdulhameed [71], studying the equilibrium is important because it explains the adsorption mechanism and the affinity between the adsorbent and adsorbate. Various temperatures were used to obtain the isotherms through Langmuir, Freundlich, Sips and Redlich–Peterson models. Fig. 7 depicts the isotherms and Table 4 presents the model parameters.

Fig. 7 illustrates the investigation of the adsorption capacity in relation to the initial DFS concentration, using EWB as an adsorbent at three temperatures (295, 305 and 315 K). An increase in the DFS adsorption was observed with the increase of initial DFS concentrations ranging from 3 to 21 mg $L^{-1}$. At low initial DFS concentration, the availability of adsorption sites was relatively high and the drug was easily adsorbed, whereas, at high initial DFS concentration, the number of available sites decreased. This happens because of the increase in the driving force from the concentration gradient since the increase in the uptake at higher initial DFS concentration is a result of the greater availability of DFS ions in the solution and then more sorption will occur [58,72]. Lastly, the maximum uptake was 42.08 mg $g^{-1}$, indicating a great efficiency for DFS removal.

Changes in temperature affect the diffusion molecules and change the equilibrium capacity of the adsorbent for a specific adsorbate [73]. Fig. 7 shows that the temperature had an important influence on DFS uptake, since the maximum adsorption capacity increased from 30.74 to 42.08 mg $g^{-1}$ while the temperature increased from 295 to 305 K, using the best initial DFS concentration obtained in Box–Behnken experimental design (15 mg $L^{-1}$). This behavior indicates an endothermic nature [74]. Table 4 presents the model parameters obtained for each isotherm.

The Sips isotherm best-fit the data for all temperatures, having the highest $R^2$ values. This most probably happens because of the complexity of the Sips equation, which better describes the heterogeneous surface [6]. Although the Redlich–Peterson isotherm also showed a good fit considering the high $R^2$ and low SD values, the Sips isotherm showed the best fit. This model predicts that for low DFS concentrations, the data follows the Freundlich model, whereas, for higher DFS concentrations, it follows the Langmuir model. The best fit for the Sips isotherm was reported in various studies, such as sludge-based activated carbons [75], modified biochar from *Moringa* seed powder [34], activated carbons and polymeric resin [76], and commercial organoclay [6].

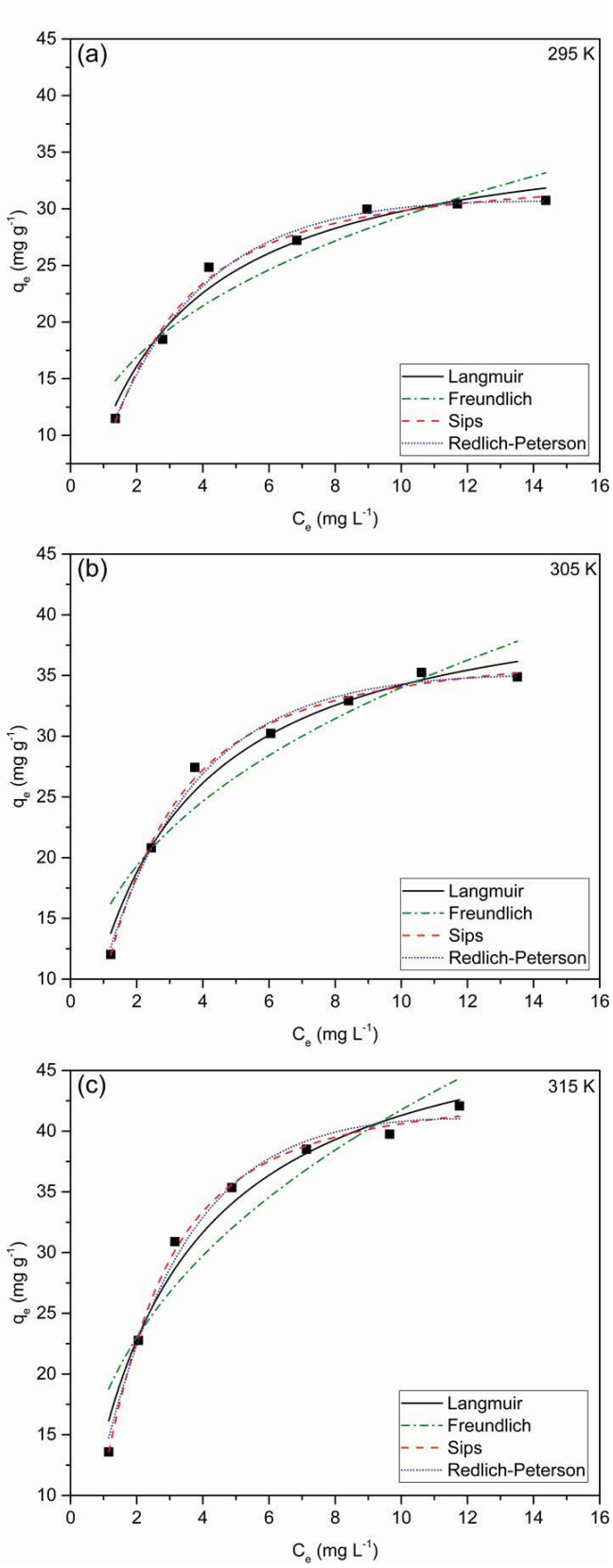


Fig. 7. Adsorption isotherms for DFS on EWB at (a) 295 K, (b) 305 K and (c) 315 K. Conditions: stirring rate = 185 rpm; pH = 5.5 (natural); contact time = 6 h; adsorbent dosage = 10 mg.

Table 4
Isotherm parameters for DFS adsorption on EWB. Conditions: stirring rate = 185 rpm; pH = 5.5 (natural); contact time = 6 h; adsorbent dosage = 10 mg

| Model | Parameters | 295 K | 305 K | 315 K |
|---|---|---|---|---|
| Langmuir | $q_{exp}$ (mg g$^{-1}$) | 30.38 | 34.35 | 40.11 |
| | $q_{max}$ (mg g$^{-1}$) | 37.81 | 43.09 | 51.82 |
| | $K_L$ (L mg$^{-1}$) | 0.3702 | 0.3855 | 0.3923 |
| | $R^2$ | 0.9718 | 0.9759 | 0.9713 |
| | SD | 1.220 | 1.322 | 1.751 |
| Freundlich | $K_F$ ((mg g$^{-1}$)(mg L$^{-1}$)$^{-1/nF}$) | 13.35 | 15.13 | 17.80 |
| | $n_F$ | 2.928 | 2.843 | 2.700 |
| | $R^2$ | 0.8784 | 0.8865 | 0.8845 |
| | SD | 2.533 | 2.869 | 3.511 |
| Sips | $q_{max}$ (mg g$^{-1}$) | 33.13 | 37.44 | 43.45 |
| | $K_S$ (L mg$^{-1}$) | 0.3264 | 0.3543 | 0.3609 |
| | $n_S$ | 0.6935 | 0.6865 | 0.6253 |
| | $R^2$ | 0.9857 | 0.9908 | 0.9952 |
| | SD | 0.8679 | 0.8164 | 0.7163 |
| Redlich–Peterson | $K_{RP}$ (mg g$^{-1}$) | 9.993 | 12.41 | 14.81 |
| | $\alpha_{RP}$ (L mg$^{-1}$) | 0.1236 | 0.1523 | 0.1324 |
| | $B$ | 1.274 | 1.235 | 1.298 |
| | $R^2$ | 0.9873 | 0.9869 | 0.9859 |
| | SD | 0.8158 | 0.9763 | 1.226 |

The increase of the temperature caused both $K_S$ and $n_S$ constant values to rise, indicating the favorable behavior at higher temperatures [77]. The higher the $K_S$ values are, the stronger the affinity is between EWB and DFS [78,79]. Increasing the temperature results in the raising of the $K_S$ parameter, which means that the adsorption capacity is favorable at higher temperatures, evidencing the endothermic process. The $n_S$ constant values (0.693, 0.686 and 0.625) suggest that the adsorption process closely resembles the monolayer model ($n_S > 0.5$) [79], indicating that the behavior is more similar to the Langmuir isotherm.

Comparing the classic isotherm models, it is possible to note that the Langmuir model best fit the experimental data, with an $R^2$ value closer to the unit and lower SD values, while for the Freundlich model, the $R^2$ values did not reach 0.9 and the SD values were higher than the other models. Furthermore, the adsorption capacity obtained through the Langmuir model was closer to the experimental value, showing conformity with the data obtained during the adsorption process. It can also be affirmed that the adsorption process of DFS on EWB occurs based on the Langmuir model, implying that the adsorption occurs as a monolayer mechanism on a homogeneous surface, which assumes that all sites are identical and limited, without any interaction between the adsorbed molecules [36,70].

The DFS adsorption capacity through the Langmuir model obtained in this study was compared to other studies found in the literature (Table 5).

The maximum adsorption capacity obtained in this study showed to be similar to some of the studies performed for DFS removal. Although the adsorption capacity obtained in this study using EWB as adsorbent was lower than some obtained in other studies using different adsorbents, such as sugar cane bagasse-derived activated carbon [81] and magnetic amine-functionalized chitosan [82], it was still better compared to other adsorbents, such as polymeric resin [76] and commercial organoclay [6]. Considering that a natural and renewable adsorbent was used (Eucalyptus wood biochar), the results obtained in this study showed that the adsorption process of DFS on EWB was efficient.

### 3.3.3. Thermodynamic study

Through the thermodynamic study, as well as its characteristics and parameters ($\Delta G$, $\Delta H$ and $\Delta S$), it is possible to explore the adsorption feasibility, capacity, and rate, as well as its nature and type [83,84]. Eq. (11) was employed to calculate $\Delta G$ and, by plotting the graph $\ln K_S \times 1/T$ obtained from Eq. (12), it was possible to determine $\Delta H$ and $\Delta S$ parameters through the regression and linear correlation coefficients, respectively. Table 6 presents the thermodynamic parameters. The negative $\Delta G$ values imply that the DFS adsorption on EWB is spontaneous with a great affinity between them [39]. Also, the increase in the temperature decreases the $\Delta G$ values, suggesting that the process is favorable at higher temperatures [85].

The positive $\Delta H$ value (3.97 kJ mol$^{-1}$) confirms the endothermic nature [86], supporting the results of the equilibrium study, since increasing the temperature will raise the DFS uptake. The $\Delta H$ magnitude obtained in this study (<40 kJ mol$^{-1}$) suggests that the DFS removal can be described by physical adsorption [87]. As discussed above in Sections 3.1 – Adsorbent characterization and 3.2.1 – Influence of pH regarding the FTIR analysis and the

Table 5
Langmuir adsorption capacity of DFS using different adsorbents

| Adsorbent | Temperature | $q_m$ | $K_L$ | $R^2$ | Reference |
|---|---|---|---|---|---|
| | (K) | (mg $g^{-1}$) | (L $mg^{-1}$) | | |
| EWB | 295 | 37.81 | 0.3702 | 0.9718 | This work |
| | 305 | 43.09 | 0.3855 | 0.9759 | |
| | 315 | 51.82 | 0.3923 | 0.9713 | |
| Commercial organoclay | 288 | 25.47 | 0.005 | 0.96 | [6] |
| | 303 | 34.06 | 0.207 | 0.92 | |
| | 323 | 39.39 | 0.628 | 0.94 | |
| Lignin-porous biochar containing graphitic carbon | 298 | 159.7 | 0.25 | 0.98 | [80] |
| | 308 | 165.9 | 0.52 | 0.96 | |
| | 318 | 195.1 | 0.21 | 0.98 | |
| Pristine biochar | 298 | 35.2 | 0.36 | 0.93 | [80] |
| | 308 | 37.4 | 0.33 | 0.96 | |
| | 318 | 46.3 | 0.30 | 0.98 | |
| Sugarcane bagasse-derived activated carbon | 298 | 315.0 | 0.0987 | 0.989 | [81] |
| Polymeric resin | 298 | 36.90 | 0.084 | 0.9959 | [76] |
| Magnetic amine-functionalized chitosan | 303.2 | 469.48 | 0.021 | 0.958 | [82] |

Table 6
Thermodynamic parameters for DFS adsorption on EWB

| $\Delta G$ (kJ $mol^{-1}$) | | | $\Delta H$ | $\Delta S$ |
|---|---|---|---|---|
| 22°C | 32°C | 42°C | (kJ $mol^{-1}$) | (kJ $mol^{-1}$ $K^{-1}$) |
| –28.16 | –29.33 | –30.34 | 3.97 | 0.109 |

influence of pH, hydrogen bondings and Van der Waals forces can be mentioned as the main adsorption mechanisms for DFS adsorption on EWB. These are considered physical and non-covalent interactions between the adsorbent and the adsorbate [88,89], agreeing with the enthalpy value (3.97 kJ $mol^{-1}$). Other interactions of a physical nature were pointed out as an adsorption mechanism for DFS removal [90]. The positive $\Delta S$ value (0,109 kJ $mol^{-1}$ $K^{-1}$) suggests that randomness in the solid-solution interface increases during the process [91], which means that the adsorbed molecules will gain more translational entropy than the adsorbate ions can lose, and the randomness of the system will remain [92].

## 4. Conclusion

Eucalyptus wood biochar was explored as a cheap material for DFS removal. SEM images showed a porous structure distributed across the surface. $N_2$ adsorption/desorption isotherm showed a high $N_2$ adsorption, with a hysteresis loop, superficial surface area of 619.13 $m^2$ $g^{-1}$ and average pore size of 3.617 nm. Batch tests showed that the best pH condition was found to be 5, at a contact time of 6 h and a temperature of 315 K. For RSM, the optimal parameters were 183.84 rpm for the stirring rate, 15 mg $g^{-1}$ for the initial DFS concentration and 10 mg for the adsorbent dosage. As for the kinetic study, the pseudo-second-order model best fit the experimental data, and the Sips model best fit the data for the equilibrium study. Through the thermodynamic parameters, the adsorption process was spontaneous and endothermic. The maximum adsorption capacity obtained was 42.08 mg $g^{-1}$. Finally, EWB has shown effective results on DFS adsorption, which means that this adsorbent is a promising and economic alternative for DFS removal.

## Acknowledgments

This work was supported financially by the Higher Education Personnel Improvement Coordination (CAPES) under Grant [88882.441557/2019–01] and National Counsel of Technological and Scientific Development (CNPq) under Grant [487115/2013–9].

## References

[1] V. Lozano-Morales, I. Gardi, S. Nir, T. Undabeytia, Removal of pharmaceuticals from water by clay-cationic starch sorbents, J. Cleaner Prod., 190 (2018) 703–711.
[2] M. Cantarella, S.C. Carroccio, S. Dattilo, R. Avolio, R. Castaldo, C. Puglisi, V. Privitera, Molecularly imprinted polymer for selective adsorption of diclofenac from contaminated water, Chem. Eng. J., 367 (2019) 180–188.
[3] J.-Q. Xiong, M.B. Kurade, B.-H. Jeon, Can microalgae remove pharmaceutical contaminants from water?, Trends Biotechnol., 36 (2018) 30–44.
[4] X. Lu, Y. Shao, N. Gao, J. Chen, Y. Zhang, Q. Wang, Y. Lu, Adsorption and removal of clofibric acid and diclofenac from water with MIEX resin, Chemosphere, 161 (2016) 400–411.
[5] S. Li, J. Cui, X. Wu, X. Zhang, Q. Hu, X. Hou, Rapid in situ microwave synthesis of $Fe_3O_4$@MIL-100(Fe) for aqueous diclofenac sodium removal through integrated adsorption and photodegradation, J. Hazard. Mater., 373 (2019) 408–416.
[6] G.S. Maia, J.R. Andrade, M.G.C. da Silva, M.G.A. Vieira, Adsorption of diclofenac sodium onto commercial organoclay: kinetic, equilibrium and thermodynamic study, Powder Technol., 345 (2019) 140–150.
[7] J.L. Sotelo, G. Ovejero, A. Rodríguez, S. Álvarez, J. Galán, J. García, Competitive adsorption studies of caffeine and

diclofenac aqueous solutions by activated carbon, Chem. Eng. J., 240 (2014) 443–453.
[8] N. Nakada, H. Shinohara, A. Murata, K. Kiri, S. Managaki, N. Sato, H. Takada, Removal of selected pharmaceuticals and personal care products (PPCPs) and endocrine-disrupting chemicals (EDCs) during sand filtration and ozonation at a municipal sewage treatment plant, Water Res., 41 (2007) 4373–4382.
[9] C. Sheng, A.G.A. Nnanna, Y. Liu, J.D. Vargo, Removal of trace pharmaceuticals from water using coagulation and powdered activated carbon as pretreatment to ultrafiltration membrane system, Sci. Total Environ., 550 (2016) 1075–1083.
[10] R. Liang, J.C. Van Leuwen, L.M. Bragg, M.J. Arlos, L.C.M. Li Chun Fong, O.M. Schneider, I. Jaciw-Zurakowsky, A. Fattahi, S. Rathod, P. Peng, M.R. Servos, Y.N. Zhou, Utilizing UV-LED pulse width modulation on $TiO_2$ advanced oxidation processes to enhance the decomposition efficiency of pharmaceutical micropollutants, Chem. Eng. J., 361 (2019) 439–449.
[11] N. Vieno, T. Tuhkanen, L. Kronberg, Removal of pharmaceuticals in drinking water treatment: effect of chemical coagulation, Environ. Technol., 27 (2006) 183–192.
[12] B.N. Bhadra, P.W. Seo, S.H. Jhung, Adsorption of diclofenac sodium from water using oxidized activated carbon, Chem. Eng. J., 301 (2016) 27–34.
[13] A. Azari, B. Kakavandi, R.R. Kalantary, E. Ahmadi, M. Gholami, Z. Torkshavand, M. Azizi, Rapid and efficient magnetically removal of heavy metals by magnetite-activated carbon composite: a statistical design approach, J. Porous Mater., 22 (2015) 1083–1096.
[14] R.R. Kalantry, A.J. Jafari, A. Esrafili, B. Kakavandi, A. Gholizadeh, A. Azari, Optimization and evaluation of reactive dye adsorption on magnetic composite of activated carbon and iron oxide, Desal. Water Treat., 57 (2015) 6411–6422.
[15] M.S. Rahaman, A. Basu, M.R. Islam, The removal of As(III) and As(V) from aqueous solutions by waste materials, Bioresour. Technol., 99 (2008) 2815–2823.
[16] M. Massoudinejad, A. Asadi, M. Vosoughi, M. Gholami, B. Kakavandi, M.A. Karami, A comprehensive study (kinetic, thermodynamic and equilibrium) of arsenic(V) adsorption using $KMnO_4$ modified clinoptilolite, Korean J. Chem. Eng., 32 (2015) 2078–2086.
[17] M. Ahmaruzzaman, Adsorption of phenolic compounds on low-cost adsorbents: a review, Adv. Colloid Interface Sci., 143 (2008) 48–67.
[18] D.D. Sewu, P. Boakye, S.H. Woo, Highly efficient adsorption of cationic dye by biochar produced with Korean cabbage waste, Bioresour. Technol., 224 (2016) 206–213.
[19] H.N. Tran, S.J. You, H.P. Chao, Fast and efficient adsorption of methylene green 5 on activated carbon prepared from new chemical activation method, J. Environ. Manage., 188 (2017) 322–336.
[20] M. Ahmadi, H. Rahmani, B. Ramavandi, B. Kakavandi, Removal of nitrate from aqueous solution using activated carbon modified with Fenton reagents, Desal. Water Treat., 76 (2017) 265–275.
[21] S. Rovani, M.T. Censi, S.L. Pedrotti, É.C. Lima, R. Cataluña, A.N. Fernandes, Development of a new adsorbent from agro-industrial waste and its potential use in endocrine disruptor compound removal, J. Hazard. Mater., 271 (2014) 311–320.
[22] K. Sen, J.K. Datta, N.K. Mondal, Glyphosate adsorption by *Eucalyptus camaldulensis* bark-mediated char and optimization through response surface modeling, Appl. Water Sci., 9 (2019) 162, doi: 10.1007/s13201-019-1036-3.
[23] A.A. Babaei, S.N. Alavi, M. Akbarifar, K. Ahmadi, A.R. Esfahani, B. Kakavandi, Experimental and modeling study on adsorption of cationic methylene blue dye onto mesoporous biochars prepared from agrowaste, Desal. Water Treat., 57 (2016) 27199–27212.
[24] Z. Aksu, Application of biosorption for the removal of organic pollutants: a review, Process Biochem., 40 (2005) 997–1026.
[25] IBÁ, Relatório anual 2017, Indústria Brasileira de Árvores – IBÁ, 2018. Available at: https://iba.org/datafiles/publicacoes/relatorios/iba-relatorioanual2019.pdf (accessed 25 March 2020).
[26] J.R. Regalbuto, J.O. Robles, The Engineering of Pt/Carbon Catalyst Preparation, University of Illinois, Chicago, 2004.
[27] S. Lagergren, Zur theorie der sogenannten adsorption gelöster stoffe, Kungliga Svenska Vetenskapsakademiens, Handlingar, 24 (1898) 1–39.
[28] Y.S. Ho, G. McKay, Pseudo-second-order model for sorption processes, Process Biochem., 34 (1999) 451–465.
[29] W.J. Weber, J.C. Morris, Kinetics of adsorption on carbon from solution, J. Sanit. Eng. Div., 89 (1963) 31–60.
[30] I. Langmuir, The constitution and fundamental properties of solids and liquids. Part I. Solids, J. Am. Chem. Soc., 38 (1916) 2221–2295.
[31] H. Freundlich, Over the adsorption in solution, J. Phys. Chem., 57 (1906) 385–470.
[32] R. Sips, On the structure of a catalyst surface, J. Chem. Phys., 16 (1948) 490–495, doi: 10.1063/1.1746922.
[33] O. Redlich, D.L. Peterson, A useful adsorption isotherm, J. Phys. Chem., 63 (1959) 1024, doi: 10.1021/j150576a611.
[34] A. Bagheri, E.A. Danso, J. Iqbal, A. Bhatnagar, Modified biochar from *Moringa* seed powder for the removal of diclofenac from aqueous solution, Environ. Sci. Pollut. Res., 27 (2020) 7318–7327.
[35] E.C. Lima, A.H. Bandegharaei, J.C.M. Piraján, I. Anastopoulos, A critical review of the estimation of the thermodynamic parameters on adsorption equilibria. Wrong use of equilibrium constant in the Van't Hoof equation for calculation of thermodynamic parameters of adsorption, J. Mol. Liq., 273 (2018) 425–434.
[36] W. Xiao, Z.N. Garba, S. Sun, I. Lawan, L. Wang, M. Lin, Z. Yuan, Preparation and evaluation of an effective activated carbon from white sugar for the adsorption of rhodamine B dye, J. Cleaner Prod., 253 (2020) 119989, doi: 10.1016/j.jclepro.2020.119989.
[37] F. Tuinstra, J.L. Koenig, Raman spectrum of graphite, J. Chem. Phys., 53 (1970) 1126–1130.
[38] O. Pezoti, A.L. Cazetta, I.P.A.F. Souza, K.C. Bedin, A.C. Martins, T.L. Silva, V.C. Almeida, Adsorption studies of methylene blue onto $ZnCl_2$-activated carbon produced from buriti shells (*Mauritia flexuosa* L.), J. Ind. Eng. Chem., 20 (2014) 4401–4407.
[39] F. Tomul, Y. Arslan, F.T. Başoğlu, Y. Babuçcuoğlu, H.N. Tran, Efficient removal of anti-inflammatory from solution by Fe-containing activated carbon: adsorption kinetics, isotherms, and thermodynamics, J. Environ. Manage., 238 (2019) 296–306.
[40] S.Á. Torrellas, A. Rodríguez, G. Ovejero, J. García, Comparative adsorption performance of ibuprofen and tetracycline from aqueous solution by carbonaceous materials, Chem. Eng. J., 283 (2016) 936–947.
[41] A.M.M. Vargas, A.L. Cazetta, C.A. Garcia, J.C.G. Moraes, E.M. Nogami, E. Lenzi, W.F. Costa, V.C. Almeida, Preparation and characterization of activated carbon from a new raw lignocellulosic material: Flamboyant (*Delonix regia*) pods, J. Environ. Manage., 92 (2011) 178–184.
[42] Q. Li, Y. Hou, X. Han, J. Wang, Y. Liu, N. Xiang, Z. Huang, Promotional effect of cyclic desulfurization and regeneration for selective catalytic reduction of NO by $NH_3$ over activated carbon, J. Cleaner Prod., 249 (2020) 119392, doi: 10.1016/j.jclepro.2019.119392.
[43] P.A. Chen, H.C. Cheng, H.P. Wang, Activated carbon recycled from bitter-tea and palm shell wastes for capacitive desalination of salt water, J. Cleaner Prod., 174 (2018) 927–932.
[44] S.S. Lam, E. Azwar, W. Peng, Y.F. Tsang, N.L. Ma, Z. Liu, Y.K. Park, E.E. Kwon, Cleaner conversion of bamboo into carbon fibre with favourable physicochemical and capacitive properties via microwave pyrolysis combining with solvent extraction and chemical impregnation, J. Cleaner Prod., 236 (2019) 117692, doi: 10.1016/j.jclepro.2019.117692.
[45] C. Saucier, M.A. Adebayo, E.C. Lima, R. Cataluña, P.S. Thue, L.D.T. Prola, M.J. Puchana-Rosero, F.M. Machado, F.A. Pavan, G.L. Dotto, Microwave-assisted activated carbon from cocoa shell as adsorbent for removal of sodium diclofenac and nimesulide from aqueous effluents, J. Hazard. Mater., 289 (2015) 18–27.
[46] S. Storck, H. Bretinger, W.F. Maier, Characterization of micro- and mesoporous solids by physisorption methods and pore-size analysis, Appl. Catal., A, 174 (1998) 137–146.

[47] M. Thommes, K. Kaneko, A.V. Neimark, J.P. Olivier, F.R. Reinoso, J. Rouquerol, K.S.W. Sing, Physisorption of gases, with special reference to the evaluation of surface area and pore size distribution (IUPAC Technical Report), Pure Appl. Chem., 87 (2015), doi: 10.1515/pac-2014–1117.
[48] A. Fini, C. Cavallari, G. Bassini, F. Ospitali, R. Morigi, Diclofenac salts, Part 7: are the pharmaceutical salts with aliphatic amines stable?, J. Pharm. Sci., 101 (2012) 3157–3168.
[49] S.K. Bajpai, M. Bhowmik, Adsorption of diclofenac sodium from aqueous solution using polyaniline as a potential sorbent. I. Kinetic studies, J. Appl. Polym. Sci., 117 (2010) 3615–3622.
[50] A.C.S. Guerra, M.B. Andrade, T.R.T. Santos, R. Bergamasco, Adsorption of sodium diclofenac in aqueous medium using graphene oxide nanosheets, Environ. Technol., 30 (2019) 1–11.
[51] L.R. Rad, M. Irani, R. Barzegar, Adsorptive removal of acetaminophen and diclofenac using NaX nanozeolites synthesized by microwave method, Korean J. Chem. Eng., 32 (2015) 1606–1612.
[52] M. Bernardo, S. Rodrigues, N. Lapa, I. Matos, F. Lemos, M.K.S. Batista, A.P. Carvalho, I. Fonseca, High efficacy on diclofenac removal by activated carbon produced from potato peel waste, Int. J. Environ. Sci. Technol., 13 (2016) 1989–2000.
[53] J.R. Domínguez, T. González, P. Palo, E.M.C. Correa, Removal of common pharmaceuticals present in surface waters by Amberlite XAD-7 acrylic-ester-resin: influence of pH and presence of other drugs, Desalination, 269 (2011) 231–238.
[54] R. Baccar, M. Sarrà, J. Bouzid, M. Feki, P. Blánquez, Removal of pharmaceutical compounds by activated carbon prepared from agricultural by-product, Chem. Eng. J., 211–212 (2012) 310–317.
[55] P.N. Panahi, D. Salari, A. Niaei, S.M. Mousavi, NO reduction over nanostructure M-Cu/ZSM-5 (M: Cr, Mn, Co and Fe) bimetallic catalysts and optimization of catalyst preparation by RSM, J. Ind. Eng. Chem., 19 (2013) 1793–1799.
[56] Y. Huang, Y. Yuan, Z. Zhou, J. Liang, Z. Chen, G. Li, Optimization and evaluation of chelerythrine nanoparticles composed of magnetic multiwalled carbon nanotubes by response surface methodology, Appl. Surf. Sci., 292 (2014) 378–386.
[57] A.K. Sood, R.K. Ohdar, S.S. Mahapatra, Parametric appraisal of mechanical property of fused deposition modelling processed parts, Mater. Des., 31 (2010) 287–295.
[58] Y. Tang, L. Chen, X. Wei, Q. Yao, T. Li, Removal of lead ions from aqueous solution by the dried aquatic plant, *Lemna perpusilla* Torr, J. Hazard. Mater., 244–245 (2013) 603–612.
[59] J. Tang, Y. Li, X. Wang, M. Daroch, Effective adsorption of aqueous $Pb^{2+}$ by dried biomass of *Landoltia punctata* and *Spirodela polyrhiza*, J. Cleaner Prod., 145 (2017) 25–34.
[60] A. Shukla, Y.H. Zhang, P. Dubey, J.L. Margrave, S.S. Shukla, The role of sawdust in the removal of unwanted materials from water, J. Hazard. Mater., 95 (2002) 137–152.
[61] L.J. Yu, S.S. Shukla, K.L. Dorris, A. Shukla, J.L. Margrave, Adsorption of chromium from aqueous solutions by maple sawdust, J. Hazard. Mater. 100 (2003) 53–63.
[62] S. Zhuang, R. Cheng, M. Kang, J. Wang, Kinetic and equilibrium of U(VI) adsorption onto magnetic amidoxime-functionalized chitosan beads, J. Cleaner Prod., 188 (2018) 655–661.
[63] A.A. Mir, A.A. Amooey, S. Ghasemi, Adsorption of direct yellow 12 from aqueous solutions by an iron oxide-gelatin nanoadsorbent; kinetic, isotherm and mechanism analysis, J. Cleaner Prod., 170 (2018) 570–580.
[64] C. Saucier, P. Karthickeyan, V. Ranjithkumar, E.C. Lima, G.S. dos Reis, I.A.S. de Brum, Efficient removal of amoxicillin and paracetamol from aqueous solutions using magnetic activated carbon, Environ. Sci. Pollut. Res., 24 (2017) 5918–5932.
[65] S. Wong, H.H. Tumari, N. Ngadi, N.B. Mohamed, O. Hassan, R. Mat, S.N.A.S. Amin, Adsorption of anionic dyes on spent tea leaves modified with polyethyleneimine (PEI-STL), J. Cleaner Prod., 206 (2019) 394–406.
[66] E. Guibal, P. McCarrick, J.M. Tobin, Comparison of the sorption of anionic dyes on activated carbon and chitosan derivatives from dilute solutions, Sep. Sci. Technol., 38 (2003) 3049–3073.
[67] A. Özcan, E.M. Öncü, A.S. Özcan, Adsorption of Acid Blue 193 from aqueous solutions onto DEDMA-sepiolite, J. Hazard. Mater., 129 (2006) 244–252.
[68] J.A. Kumar, D.J. Amarnath, S.A. Jabasingh, P.S. Kumar, K.V. Anand, G. Narendrakumar, K.R.S. Namasivayam, T. Krithiga, S. Sunny, S.P. Pushkala, D. Yuvarajan, One pot green synthesis of nano magnesium oxide-carbon composite: preparation, characterization and application towards anthracene adsorption, J. Cleaner Prod., 237 (2019) 117691, doi: 10.1016/j.jclepro.2019.117691.
[69] L. Qiao, S. Li, Y. Li, Y. Liu, K. Du, Fabrication of superporous cellulose beads via enhanced inner cross-linked linkages for high efficient adsorption of heavy metal ions, J. Cleaner Prod., 253 (2020) 120017, doi: 10.1016/j.jclepro.2020.120017.
[70] B.H. Hameed, D.K. Mahmoud, A.L. Ahmad, Equilibrium modeling and kinetic studies on the adsorption of basic dye by a low-cost adsorbent: coconut (*Cocos nucifera*) bunch waste, J. Hazard. Mater., 158 (2008) 65–72.
[71] A.S. Abdulhameed, A.T. Mohammad, A.H. Jawad, Application of response surface methodology for enhanced synthesis of chitosan tripolyphosphate/$TiO_2$ nanocomposite and adsorption of reactive orange 16 dye, J. Cleaner Prod., 232 (2019) 43–56.
[72] N. Tewari, P. Vasudevan, B.K. Guha, Study on biosorption of Cr(VI) by *Mucor hiemalis*, Biochem. Eng. J., 23 (2005) 185–192.
[73] M. Doğan, M. Alkan, Ö. Demirbaş, Y. Özdemir, C. Özmetin, Adsorption kinetics of maxilon blue GRL onto sepiolite from aqueous solutions, Chem. Eng. J., 124 (2006) 89–101.
[74] A. Mittal, L. Krishnan, V.K. Gupta, Removal and recovery of malachite green from wastewater using an agricultural waste material, de-oiled soya, Sep. Purif. Technol., 43 (2005) 125–133.
[75] G.C. Reis, B.M.K. Mahbub, M. Wilhelm, E.C. Lima, C.H. Sampaio, C. Saucier, P.S.L. Dias, Activated carbon from sewage sludge for removal of sodium diclofenac and nimesulide from aqueous solutions, Korean J. Chem. Eng., 33 (2016) 3149–3161.
[76] R.N. Coimbra, C. Escapa, S. Paniagua, M. Otero, Adsorptive removal of diclofenac from ultrapure and wastewater: a comparative assessment on the performance of a polymeric resin and activated carbons, Desal. Water Treat., 57 (2016) 27914–27923.
[77] K.W. Jung, B.H. Choi, M.J. Hwang, J.W. Choi, S.H. Lee, J.S. Chang, K.H. Ahn, Adsorptive removal of anionic azo dye from aqueous solution using activated carbon derived from extracted coffee residues, J. Cleaner Prod., 166 (2017) 360–368.
[78] A.L.D. Rosa, E. Carissimi, G.L. Dotto, H. Sander, L.A. Feris, Biosorption of rhodamine B dye from dyeing stones effluents using the green microalgae *Chlorella pyrenoidosa*, J. Cleaner Prod., 198 (2018) 1302–1310.
[79] N.A. Rashidi, S. Yusup, Potential of palm kernel shell as activated carbon precursors through single stage activation technique for carbon dioxide adsorption, J. Cleaner Prod., 168 (2017) 474–486.
[80] N.T.M. Tam, Y. Liu, H. Bashir, P. Zhang, S. Liu, X. Tan, M.Y. Dai, M.F. Li, Synthesis of porous biochar containing graphitic carbon derived from lignin content of forestry biomass and its application for the removal of diclofenac sodium from aqueous solution, Front. Chem., 8 (2020) 274, doi: 10.3389/fchem.2020.00274.
[81] A.O.A.E. Naga, M.E. Saied, S.A. Shaban, F.Y. El Kady, Fast removal of diclofenac sodium from aqueous solution using sugar cane bagasse-derived activated carbon, J. Mol. Liq., 285 (2019) 9–19.
[82] X.X. Liang, A.M. Omer, Z. Hu, Y. Wang, D. Yu, X. Ouyang, Efficient adsorption of diclofenac sodium from aqueous solutions using magnetic amine-functionalized chitosan, Chemosphere, 217 (2019) 270–278.
[83] C. Wei, Y. Huang, Q. Liao, A. Xia, X. Zhu, X. Zhu, Adsorption thermodynamic characteristics of *Chlorella vulgaris* with organic polymer adsorbent cationic starch: effect of temperature on adsorption capacity and rate, Bioresour. Technol., 293 (2019) 122056, doi: 10.1016/j.biortech.2019.122056.
[84] E. Wibowo, M. Rokhmat, Sutisna, Khairurrijal, M. Abdullah, Reduction of seawater salinity by natural zeolite (Clinoptilolite): adsorption isotherms, thermodynamics and kinetics, Desalination, 409 (2017) 146–156.
[85] M.A. Chayid, M.J. Ahmed, Amoxicillin adsorption on microwave prepared activated carbon from *Arundo donax* Linn:

isotherms, kinetics, and thermodynamics studies, J. Environ. Chem. Eng., 3 (2015) 1592–1601.
[86] M. Ghaedi, B. Sadeghian, A.A. Pebdani, R. Sahraei, A. Daneshfar, C. Duran, Kinetics, thermodynamics and equilibrium evaluation of direct yellow 12 removal by adsorption onto silver nanoparticles loaded activated carbon, Chem. Eng. J., 187 (2012) 133–141.
[87] D.O. Hayward, B.M.W. Trapnell, Chemisorption, 2nd ed., Butterworths, London, 1964.
[88] I. Ali, M. Asim, T.A. Khan, Low cost adsorbents for the removal of organic pollutants from wastewater, J. Environ. Manage., 113 (2012) 170–183.
[89] K. Ivanković, M. Kern, M. Rožman, Modelling of the adsorption of pharmaceutically active compounds on carbon-based nanomaterials, J. Hazard. Mater., 414 (2021) 125554, doi: 10.1016/j.jhazmat.2021.125554.
[90] R.M. Souza, H.B. Quesada, L.F. Cusioli, M.R.F. Klen, R. Bergamasco, Adsorption of non-steroidal anti-inflammatory drug (NSAID) by agro-industrial by-product with chemical and thermal modification: adsorption studies and mechanism, Ind. Crops Prod., 161 (2021) 113200, doi: 10.1016/j.indcrop.2020.113200.
[91] L. Lonappan, T. Rouissi, S.K. Brar, M. Verma, R.Y. Surampalli, An insight into the adsorption of diclofenac on different biochars: mechanisms, surface chemistry, and thermodynamics, Bioresour. Technol., 249 (2018) 386–394.
[92] P. Saha, S. Chowdhury, Insight into adsorption thermodynamics, M. Tadashi, Ed., Thermodynamics, IntechOpen, 2011, doi: 10.5772/13474.

## Supplementary information

Table S1
Characteristics and properties of DFS

| | |
|---|---|
| Molecular formula | $C_{14}H_{10}Cl_2NNaO_2$ |
| CAS | 15307-79-6 |
| Molecular weight (g mol$^{-1}$) | 318.13[a] |
| Acid dissociation constant (pKa) | 4.15[a] |
| Solubility in water (mg L$^{-1}$) | 2,430[a] |
| Molecule size (nm) | 1.01 × 0.719 × 0.484[b] |

[a][S1], [b][S2]

Table S4
BBD optimal conditions for DFS adsorption onto EWB

| Parameter | Optimal condition | Actual $q_e$ (mg g$^{-1}$) |
|---|---|---|
| Stirring rate (rpm) | 183.8 | |
| Drug concentration (mg L$^{-1}$) | 15.0 | 31.78 |
| Adsorbent dosage (mg) | 10.0 | |

Table S2
BBD matrix of the predicted and actual DFS adsorption onto EWB

| Run | Stirring rate ($X_1$) | Drug concentration ($X_2$) | Adsorbent dosage ($X_3$) | Actual value | Predicted value |
|---|---|---|---|---|---|
| 1 | 100 (–1) | 5 (–1) | 20 (0) | 9.317 | 8.480 |
| 2 | 200 (+1) | 5 (–1) | 20 (0) | 11.49 | 11.46 |
| 3 | 100 (–1) | 15 (+1) | 20 (0) | 18.90 | 18.93 |
| 4 | 200 (+1) | 15 (+1) | 20 (0) | 24.77 | 25.60 |
| 5 | 100 (–1) | 10 (0) | 10 (–1) | 17.78 | 18.68 |
| 6 | 200 (+1) | 10 (0) | 10 (–1) | 25.23 | 25.32 |
| 7 | 100 (–1) | 10 (0) | 30 (+1) | 11.39 | 11.30 |
| 8 | 200 (+1) | 10 (0) | 30 (+1) | 15.20 | 14.31 |
| 9 | 150 (0) | 5 (–1) | 10 (–1) | 18.09 | 18.03 |
| 10 | 150 (0) | 15 (+1) | 10 (–1) | 30.51 | 29.59 |
| 11 | 150 (0) | 5 (–1) | 30 (+1) | 7.168 | 8.094 |
| 12 | 150 (0) | 15 (+1) | 30 (+1) | 21.07 | 21.13 |
| 13 | 150 (0) | 10 (0) | 20 (0) | 20.49 | 20.54 |
| 14 | 150 (0) | 10 (0) | 20 (0) | 20.92 | 20.54 |
| 15 | 150 (0) | 10 (0) | 20 (0) | 20.18 | 20.54 |

Table S3
Analysis of variance (ANOVA) for DFS adsorption onto EWB

| Source | DF | SS (Aj.) | MS (Aj.) | *F*-value | Prob. > *F* | |
|---|---|---|---|---|---|---|
| Model | 9 | 565.694 | 62.855 | 62.59 | 0.000 | Significant |
| $X_1$ | 1 | 46.592 | 46.592 | 46.39 | 0.001 | Significant |
| $X_2$ | 1 | 302.393 | 302.393 | 301.09 | 0.000 | Significant |
| $X_3$ | 1 | 169.172 | 169.172 | 168.45 | 0.000 | Significant |
| $X_1^2$ | 1 | 35.760 | 35.760 | 35.61 | 0.002 | Significant |
| $X_2^2$ | 1 | 6.276 | 6.276 | 6.25 | 0.055 | |
| $X_3^2$ | 1 | 0.002 | 0.002 | 0.00 | 0.967 | |
| $X_1X_2$ | 1 | 3.400 | 3.400 | 3.39 | 0.125 | |
| $X_1X_3$ | 1 | 3.305 | 3.305 | 3.29 | 0.129 | |
| $X_2X_3$ | 1 | 0.544 | 0.544 | 0.54 | 0.495 | |
| Lack of fit | 3 | 4.747 | 1.582 | 11.54 | 0.081 | Not significant |
| Pure error | 2 | 0.274 | 0.137 | * | * | |
| Total | 14 | 570.716 | | | | |
| $R^2 = 0.9912$ | | | | | | |

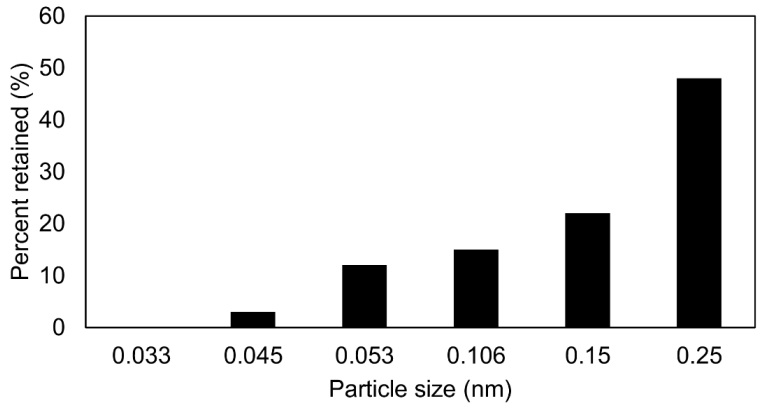


Fig. S1. Effect of EWB particle size.

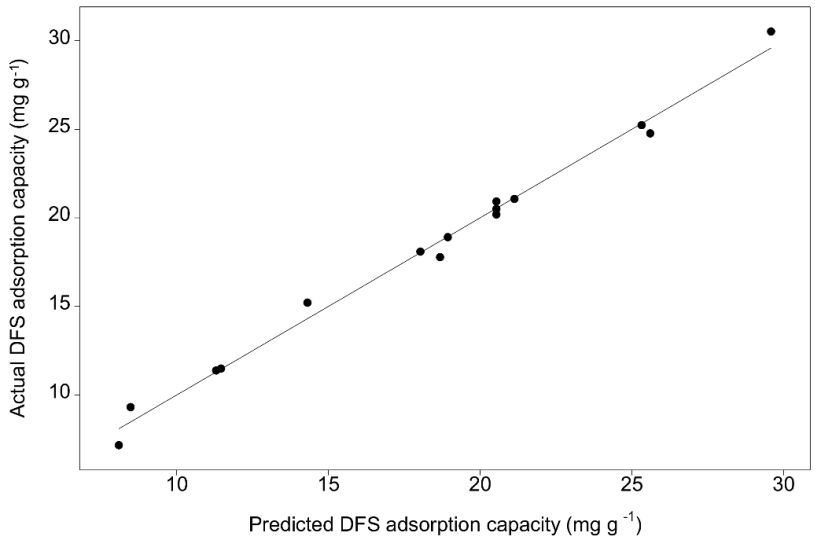


Fig. S2. The actual and predicted plots for DFS uptake capacity onto EWB.

## References

[S1] S.A. Torrellas, R.G. Lovera, N. Escalona, C. Sepúlveda, J.L. Sotelo, J. García, Chemical-activated carbons from peach stones for the adsorption of emerging contaminants in aqueous solutions, Chem. Eng. J., 279 (2015) 788–798.

[S2] M. Bernardo, S. Rodrigues, N. Lapa, I. Matos, F. Lemos, M.K.S. Batista, A.P. Carvalho, I. Fonseca, High efficacy on diclofenac removal by activated carbon produced from potato peel waste, Int. J. Environ. Sci. Technol., 13 (2016) 1989–2000.